*J. Fluid Mech.* (1978), *vol.* 89, *part* 1, *pp.* 1–31
*Printed in Great Britain*



# Large-scale motion in a turbulent boundary layer: a study using temperature contamination

By CHYAN-HAI P. CHEN† AND RON F. BLACKWELDER
Department of Aerospace Engineering, University of Southern California, Los Angeles

(Received 28 February 1977)

A fully developed turbulent boundary layer with a zero pressure gradient was explored by using temperature as a passive contaminant in order to study the large-scale structure. The temperature tracer was introduced into the flow field by heating the entire wall to approximately 12 °C above the free-stream temperature. The most interesting observation was the existence of a sharp internal temperature front, characterized by a rapid decrease in temperature, that extended throughout the entire boundary layer. In the outer, intermittent region, the internal temperature front was always associated with the upstream side of the turbulent bulges, i.e. the 'backs'. It extended across the entire logarithmic region and was related to the sharp acceleration associated with the bursting phenomenon near the wall. Conditional averages of the velocities measured with the temperature front revealed that it was associated with an internal shear layer. The results suggest that this shear layer provides a dynamical relationship between the large structures in the outer, intermittent region and the bursting phenomenon near the wall.

## 1. Introduction

In the past decade, quasi-ordered structures have been found to play an important role in the dynamics of nearly all turbulent shear flows, as discussed by Laufer (1975). Large-scale eddy motions have been observed in many basic free turbulent flows. Some examples include the observations in mixing layers by Brown & Roshko (1974) and Winant & Browand (1974), in wakes by Papailiou & Lykoudis (1974) and in jets by Rockwell & Niccols (1972). The associated sharp turbulent/non-turbulent interface has been the object of many investigations since it was first reported by Corrsin (1943) in a turbulent jet. Kaplan & Laufer (1969) and Kovasznay, Kibens & Blackwelder (1970) made extensive use of conditional sampling techniques to study the large-scale structure in the intermittent region of a boundary layer and its relationship to the turbulent/non-turbulent interface.

In a bounded turbulent shear flow, a coherent structure known as the 'bursting' phenomenon has been found to dominate the dynamics of the wall region. Its first observable manifestation is the occurrence of streamwise streaks of low speed fluid near the wall that were initially noticed by Hama (see Corrsin 1957). The lift-up and subsequent interaction of these streaks with the outer flow were first studied by Kline *et al.* (1967) in a boundary layer and by Corino & Brodkey (1969) in a pipe flow. These and other authors agree that the bursting process is responsible for most of the energy

† Present address: McDonnell Douglas Research Laboratories, St Louis, Missouri.

production in the wall region. For a more complete review of these coherent structures, the reader is referred to the articles by Kovasznay (1970), Laufer (1975) and Willmarth (1975).

Both of these two different types of ordered motion are present in a turbulent boundary layer, which has promoted some speculation about a possible relationship between them. On the basis of the findings of Kim, Kline & Reynolds (1971) and Rao, Narasimha & Badri Narayanan (1971), Laufer & Badri Narayanan (1971) showed that the normalized frequencies of occurrence $F\delta/U_\infty$ of these two different eddy structures are of the same order of magnitude and speculated that a deterministic relationship may exist between them. Kovasznay (1970) indicated that there may be a reverse cascade of eddies beginning with the small-scale 'bursts' near the wall. He suggested that they may either grow or coalesce into larger ones as they move away from the wall. These intermediate-size eddies could possibly produce large-scale eruptions owing to some instability mechanism and eventually reach the intermittent region and become visible as the turbulent bulges. The visualization studies of Nychas, Hershey & Brodkey (1973) and Offen & Kline (1974) showed that there are transverse vortices at intermediate distances from the wall. These vortices were observed to be related to some type of instability mechanism acting between the high speed fluid from the outer region and the low speed fluid from the wall layer.

The purpose of the present study was to clarify the fluid-mechanical process that relates the outer large-scale motion and the organized motion in the wall layer, and to provide quantitative measurements of this process. Thus it was decided at the outset to slightly heat the wall in order to use the temperature of the fluid as a passive contaminant. Then the fluid parcels originating near the wall had a slightly higher temperature and the fluid entrained from the free stream had a lower temperature than the average. Blackwelder & Kaplan (1976) have shown that the study of the spatial structures in turbulent shear flows is greatly facilitated by using several probes simultaneously. Therefore a rake of ten temperature-sensing probes was used. The rake had a span of $0{\cdot}6\delta$ and could be positioned either parallel or perpendicular to the wall. In this manner, simultaneous data could be obtained essentially along a line in space.

## 2. Experimental facilities and procedures

### 2.1. *Wind tunnel*

The experiments were all performed in the USC low speed wind tunnel at a nominal free-stream velocity $U_\infty = 4{\cdot}57$ m/s. The tunnel is of an open-return type which has a free-stream velocity range of 2·4–12·2 m/s. The air entered a $3{\cdot}04 \times 3{\cdot}04$ m stilling chamber, passed through four fine mesh screens, went through a 16:1 contraction into the $0{\cdot}61 \times 0{\cdot}91$ m test section and exited through a centrifugal fan to the atmosphere. The test section is 6·10 m long and has an aerodynamically smooth wall, which was used as the flat plate. The first 4·88 m of the flat plate used by Gupta, Laufer & Kaplan (1971) was replaced by two smooth aluminium plates 2·44 m long and 6·35 mm thick. The plates were carefully mated at their junction to ensure an aerodynamically smooth surface throughout. The remaining 1·22 m of the test surface consisted of a Plexiglas section, where the supporting stings of the probes were mounted. Six heat-

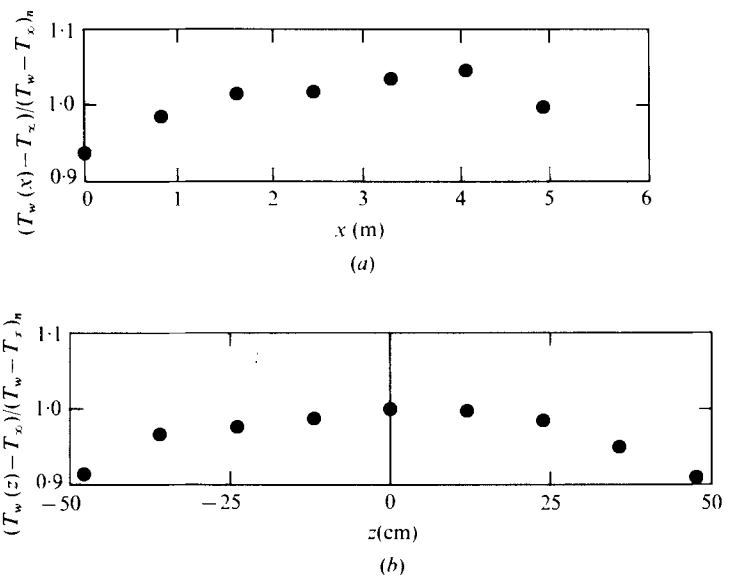


FIGURE 1. (*a*) Streamwise distribution of the mean temperature downstream from the boundary-layer trip. (*b*) Spanwise distribution of the mean temperature at the measuring station. The nominal temperature difference $(T_w - T_\infty)_n$ was 12·8 °C.

ing pads, each 81·3 × 61·0 cm, were glued onto the top of the aluminium plate, outside the tunnel. They extended from the entrance of the test section to slightly beyond the point of measurement, so that the entire boundary layer was heated along the streamwise direction. When energized by a 220 V a.c. power supply, these heating pads delivered a uniform heat flux at 98 W/m$^2$. The heating was from the top with the boundary layer on the underside of the flat plate, so that the mean flow field was stably stratified. The dynamical effects of the weak stratification were found to be negligible and thus the temperature served merely as a passive contaminant. Iron–constantan thermocouples were embedded in the exterior surface of the aluminium plate along the centre-line and in the spanwise direction at the downstream end to monitor the wall temperature. Approximately 100 min of operating time were required for the plate to reach an equilibrium temperature. Figure 1 shows the equilibrium temperature distributions on the wall in the streamwise and spanwise directions. The temperature of the flat plate was practically uniform, with nominal values of $T_w - T_\infty = 12{\cdot}8$ °C.

To ensure a zero pressure gradient through the test section, the side walls of the tunnel were slightly flared to compensate for the boundary-layer growth. The measurements were taken on the centre-line at a position 4·72 m downstream from the boundary-layer trip, which was approximately 15 cm after the entrance to the test section. The co-ordinate system is as follows: the $x$ axis is parallel to the free stream, the $y$ axis is perpendicular to the plate and the $z$ axis is perpendicular to both the $x$ and the $y$ axis according to the conventional right-hand rule.

### 2.2. *Hot-wire instrumentation*

The temperature was measured by platinum resistance thermometers which consisted essentially of a conventional constant-current anemometer operated at a very low overheat. The wires were 2·5 $\mu$m in diameter and had an aspect ratio greater than 300. When heated by 1 mA, the wire had an overheat ratio $(R_p - R_c)/R_c$ of approximately 0·005. The frequency response of the system was approximately 350 Hz as determined by the square-wave test. No compensation for the thermal lag at higher frequencies was undertaken since only the large-scale motion associated with the lower frequencies was of primary interest. Velocity contamination of the temperature signal was found to be minimal, and hence no correction was made.

A rake of resistance thermometers was used to study the coherent temperature fluctuations in the normal direction. The rake consisted of 10 identical probes spaced 6·4 mm apart. Calibration of the probes was accomplished by using a commercial hair dryer that was modified to give an air flow with a variable temperature and speed. The flow entered a styrofoam box and passed through two fine mesh screens that damped the temperature fluctuations to an imperceptible level of approximately 0·02 °C. The temperature probes were placed downstream of the screens. The flow exited through a series of holes in the styrofoam box downstream of the probes. The temperature of air in the box was monitored by an iron–constantan thermocouple with a reference junction at 0 °C. In the temperature range 20–40 °C, the resistance-thermometer responses were linear and the calibration data were digitally fitted by a least-squares method. After calibration, the temperature probes were placed in the free stream at the centre of the wind tunnel and the temperature there was recorded and used as the reference temperature $T_\infty$. Other constants measured in the free stream will also be denoted by the subscript $\infty$.

A single linearized constant-temperature hot-wire probe was used to measure the mean and fluctuation velocities in the unheated boundary layer. A triple probe, used to measure the instantaneous temperature and velocity signals, was constructed from a conventional X-probe operated in the constant-temperature mode and a resistance thermometer. The sensing element of the thermometer was directly in front of the centre of the X-probe and was perpendicular to the plane of the X-wires. The separation distance between them was less than 1 mm; hence the time delay between the temperature and velocity signals was negligible.

Each wire of the X-probe was calibrated independently by yawing the probe in the free stream to determine the coefficients $A$ and $B$ of King's law:

$$E^2 = A + B(U_\infty \cos\alpha)^{\frac{1}{2}}, \tag{1}$$

where $E$ is the output voltage of the anemometer, $U_\infty$ is the free-stream velocity and $\alpha$ is the angle between the normal to the wire and the free-stream direction. All three of these variables were recorded for various angles and velocities. It is well known that the cosine law introduces regular deviations from (1) for large angles, as discussed by Blackwelder (1979). Since these deviations are systematic, it was found that they could be incorporated in the coefficients $A$ and $B$ of (1). This was accomplished by calibrating each wire about its mean angular position ($\alpha = \pm 45°$). A least-squares fit of the calibration data obtained by varying $U_\infty$ and $\alpha$ yielded coefficients that gave negligible error over the range of velocities and flow angles of interest.

The maximum error introduced into the velocity signal by the temperature field was found to be 20% in the worst possible case. Since the fluid temperature was measured simultaneously with the triple probe, its effect on the velocity could be removed. Each instantaneous data point was corrected by using the following relationships from Corrsin (1949):

$$\frac{A}{A_\infty} = \frac{T_\infty + 125}{T + 125}\left(\frac{T}{T_\infty}\right)^{\frac{3}{2}} \frac{T_p - T}{T - T_\infty}, \tag{2}$$

$$\frac{B}{B_\infty} = \left[\frac{T_\infty + 125}{T + 125}\left(\frac{T}{T_\infty}\right)^{\frac{1}{2}}\right]^{\frac{1}{2}} \frac{T_p - T}{T - T_\infty}, \tag{3}$$

where $A_\infty$ and $B_\infty$ are the calibration constants in the free stream and $T_p$ is the temperature of the wire.

### 2.3. *Tape recorder and digital systems*

A Hewlett-Packard model 3955A fourteen-channel magnetic tape recorder was used to record the output voltages of the resistance thermometers and anemometers during calibration and the data gathering process. During recording, the tape speed was 38·1 cm/s and model 3535A FM recording amplifiers were used. When playing the signal back for digitizing, model 3537A FM output amplifiers were used and the tape speed was decreased to 4·76 cm/s to increase the digital sampling rate.

The analog outputs from the playback amplifiers were digitized at a sampling rate corresponding to 1 kHz in real time and stored on a nine-track magnetic tape for further processing. The digitizing system consisted of sixteen Datel SHM-2 sample-and-hold modules, two eight-channel Datel MM-8 analog multiplexer modules and a Datel ADC-L analog-to-digital converter. The maximum aperture and acquisition times for the sample-and-hold module were 10 ns and 100 ns, respectively, and the decay rate was $50\,\mu V/\mu s$. The input range was $\pm 5$ V and the output consisted of 11 significant bits plus one sign bit; thus the system had a quantization error of 2·5 mV, which was negligible for the type of measurement made in this study. After receiving an external timing pulse from a INTERDATA 5 minicomputer, the sample-and-hold modules sampled all the channels simultaneously. The analog signals were then multiplexed to the analog-to-digital converter. Although the converter needed only $20\,\mu s$ per channel, the sampling rate was ultimately limited by the speed of the digital tape drive, which allowed a minimum sampling interval of $150\,\mu s$ per channel.

The digital data were processed using FORTRAN IV programs by an IBM 360-44 digital computer with 256 K bytes of core. The raw data and the results were stored on magnetic disc packs and plotted on a Tektronics graphic terminal model 4010 or a CALCOMP digital incremental plotter.

## 3. Data evaluation techniques

### 3.1. *Conditional averaging in the intermittent region*

Several distinctive features were found in the temperature signals and it was deemed desirable to use conditional averaging techniques to study them. Conditional sampling requires a trigger probe whose signal is processed and used to select the members for the ensemble average. The signals to be conditionally averaged can be obtained from the trigger probe itself and/or from other probes with time delays and different spatial

locations. Following Kovasznay *et al.* (1970), the trigger signal may be a random square wave as used for zone averaging or it may be a pulse train that marks the time reference of specific events as used for point averaging.

In the outer, intermittent region, the definitions used by Kovasznay *et al.* (1970) were adopted and are briefly restated here for clarity. An intermittency function $I(\mathbf{x}, t)$ was defined by

$$I(\mathbf{x},t) = \begin{cases} 1 & \text{for turbulent flow,} \\ 0 & \text{for non-turbulent flow.} \end{cases}$$

This signal was generated by comparing the temperature signal with a threshold level. The temperature signal in the ambient, non-turbulent fluid had an r.m.s. value of approximately 0·04 °C owing to residual thermal fluctuations and electronic noise. After thoroughly studying the effect of the threshold level on the resulting statistics, it was found that a threshold of only 0·02 °C above the local non-turbulent mean temperature could be used. This low threshold did introduce some error into the results; however by using the general properties of the temperature probability density functions as explained in the appendix, the intermittency factor and the conditional averages could easily be corrected for this effect.

It is well known that intermittency functions $I(\mathbf{x}, t)$ are plagued by 'drop-outs', i.e. data points within the turbulent zone that fall below the threshold level. This problem is often alleviated by introducing a non-zero hold time, as used by Kovasznay & Ali (1974), LaRue & Libby (1974) and others. In the present study, a dual-level technique was used. This method assumed that the fluid in the turbulent zones always had a greater temperature than the local non-turbulent fluid. Once a turbulent region had been found, the intermittency function did not return to zero until the temperature was equal to or less than the local ambient temperature $T_a$. Hence the threshold level for detecting the turbulent regions was 0·02 °C above $T_a$ and was 0 °C above the ambient temperature for detecting the non-turbulent regions. The small statistical errors stemming from the 0·04 °C fluctuations in the ambient fluid were removed by the techniques described in the appendix.

The time average of $I(\mathbf{x}, t)$ yields the intermittency factor $\gamma$, which gives the fraction of the time that the probe spends in the turbulent region:

$$\gamma = \bar{I} = \lim_{T\to\infty} \frac{1}{T} \int_{t_1}^{t_1+T} I(t)\, dt. \tag{4}$$

The conventional time average of any function $Q(t)$, denoted by $\bar{Q}$, is given by

$$\bar{Q} = \lim_{T\to\infty} \frac{1}{T} \int_{t_1}^{t_1+T} Q(t)\, dt. \tag{5}$$

The zone averages in the turbulent and non-turbulent regions, $\tilde{\bar{Q}}$ and $\tilde{\bar{Q}}$, are defined as

$$\tilde{\bar{Q}} = \lim_{T\to\infty} \frac{1}{T\gamma} \int_{t_1}^{t_1+T} I(\mathbf{x},t)\, Q(t)\, dt \tag{6}$$

and

$$\tilde{\bar{Q}} = \lim_{T\to\infty} \frac{1}{(1-\gamma)\, T} \int_{t_1}^{t_1+T} (1-I)\, Q(t)\, dt. \tag{7}$$

A different type of average may be found by first defining a time sequence $t_1, t_2, t_3, \ldots, t_N$ in which every point $t_n$ denotes the temporal reference point of the event

of interest. Then the ensemble average of the quantity $Q$ related to the events is given by

$$\langle Q(\mathbf{x},\tau)\rangle_{x'} = \frac{1}{N}\sum_{n=1}^{N} Q(\mathbf{x}, t_n+\tau), \tag{8}$$

where $x$ and $x'$ denote the positions of the sampling probe and the trigger probe, respectively. The point averages $\hat{Q}$ and $\check{Q}$ used by Kovasznay *et al.* (1970) are the special cases of (8) in which $\tau = 0$ and $t_n$ is the time when the trigger probe either enters or leaves the turbulent region.

### 3.2. *Conditional averaging in the turbulent region*

In the fully turbulent region, an initial exploration indicated that a strong temperature decrease (called an 'internal temperature front') was the most obvious manifestation of a coherent structure. This rapid change in the temperature signal is quite similar to the rapid change in the velocity signals associated with the bursting phenomenon near the wall, as reported by Blackwelder & Kaplan (1976). This similarity suggested that the detection criteria of Blackwelder & Kaplan could easily be adapted to the present study with minor modifications.

The variable-interval time average (VITA) of the quantity $Q(t)$ is defined as

$$[Q(t)] = \frac{1}{T}\int_{t-\frac{1}{2}T}^{t+\frac{1}{2}T} Q(t)\,dt. \tag{9}$$

Essentially, this is a moving average which gives a local measure of the mean value of the quantity $Q$. It can be thought of as a low-pass filter which passes frequencies below $1/(2T)$ and strongly attenuates those above. The localized VITA variance of $Q$ is defined as

$$[\mathrm{var}\,(t)] = [Q^2] - [Q]^2, \tag{10}$$

which is a positive-definite quantity that emphasizes the higher frequency components of the signal $Q$. As in the method used to determine the intermittency in the outer layer, a detection function $D(t)$ can be defined as

$$D(t) = \begin{cases} 1 & \text{if} \quad [\mathrm{var}] > KQ'^2, \quad d[Q]/dt < 0, \\ 0 & \text{otherwise}, \end{cases} \tag{11}$$

where $K$ is the threshold level. Note that $Q'$ is the r.m.s. fluctuation of the quantity $Q$ at the detection location and is given by $(\lim_{T\to\infty}[\mathrm{var}])^{\frac{1}{2}}$. Blackwelder & Kaplan (1976) have shown that this criterion detects very rapid and strong changes in the quantity $Q$.

In the present investigation, the temperature signal was always used for the detection parameter $Q$. Using this technique, it was determined that there were approximately four times as many cold fronts (i.e. rapid coolings) as there were warm fronts. By observing the simultaneous temperature traces (such as that shown in figure 12) it was found that the warm fronts had very little spatial coherence and they were assumed to be associated with the random background turbulence and not with any coherent structure. Thus in order to concentrate only on the coherent structure, the additional criterion $d[Q]/dt < 0$ was added to the definition (11). The signals associated with this detection scheme are shown in figure 2.

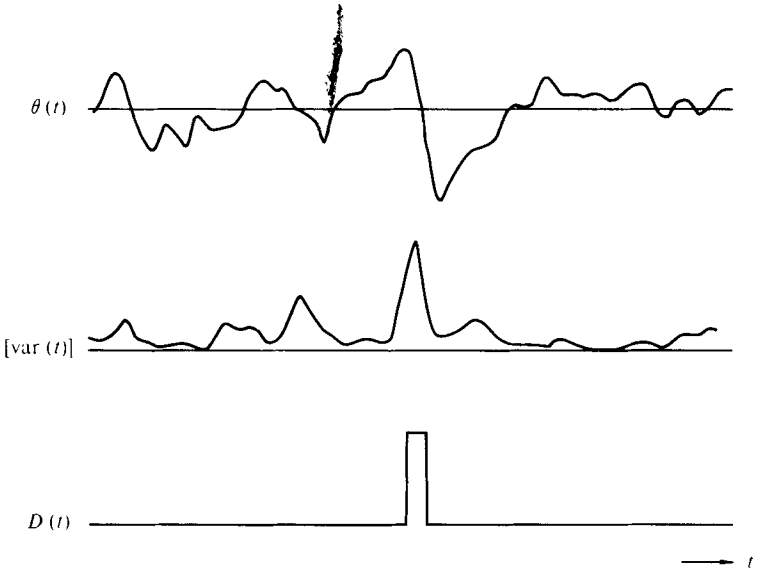


FIGURE 2. Sketch of the variable-interval time-averaging technique used for detecting the internal temperature fronts.

With the above definition, a strong temperature decrease was detected whenever $D(t)$ was 1, say from time $t_1$ to time $t_2$. The reference time $t_n$ for this event was set at the midpoint $t_n = \frac{1}{2}(t_1 + t_2)$. For each probe, a sequence of reference times was generated and used as a basis for the conditional average described by (8).

There are two free parameters in this detection scheme that must be determined: $T$ and $K$. Blackwelder & Kaplan (1976) observed that their results were rather insensitive to the averaging time $T$ over a range in which $T$ varied by a factor of two. In the present study $T$ was taken to be 5 ms, which was the average width of the cold front. A limited amount of data (2 s) was used to determine the effect of variation of $K$. It was found that $K = 0{\cdot}9$ gave the best detection of the spatial pattern by a visual comparison with the simultaneous temporal record. Both of these values are similar to those studied and used by Blackwelder & Kaplan and consequently they were used to generate the reference time series $\{t_n\}$.

### 3.3. *Coincident correlation measurement*

It was found that the internal temperature fronts were highly correlated in the $x, y$ plane. However they were skewed in space, so that the temperature front arrived later in time at the lower positions. In order to find the most probable time delay, a new technique, called coincident correlation, was developed. A sequence of time pulses $t_n$ corresponding to the passage of the fronts at the position $y$ was generated. A pulse train $P(y, t_n)$ was constructed with each pulse centred about the time $t_n$ and having a width of 5 ms, which was equal to the average width of the cold fronts. The cross-correlation between pulse trains generated at two different locations gave the average time delay between the temperature fronts at these positions. The coincident correlations are thus defined by

$$R(y_0, \Delta y, \tau) = \frac{1}{N} \sum_{n=1}^{N} \int_0^{\xi} P(y_0, t_n + s)\, P(y_0 + \Delta y, t_n + s + \tau)\, ds, \tag{12}$$

where $N$ is the number of pulses in the signal $P(y_0, t_n)$ and $\xi$ is the average period between pulses. Typically, $N$ was approximately 300 and $\xi$ was 50 ms. The time delay corresponding to the peak of the correlation function gave the most probable phase lag between the temperature fronts at $y_0$ and $y_0 + \Delta y$. The width of the pulses did affect the general shape of the correlation curve, however the locations of the peaks remained unchanged. The coincident correlation coefficient is defined as

$$C(y_0, \Delta y, \tau) = \frac{R(y_0, \Delta y, \tau) - \overline{P(y_0)}\,\overline{P(y_0 + \Delta y)}}{P'(y_0)\,P'(y_0 + \Delta y)}, \tag{13}$$

where the overbars and primes indicate conventional time average and root-mean-square values, respectively.

## 4. Results

### 4.1. *Mean velocity and temperature field*

All the measurements of temperature and velocity were performed 4·72 m downstream from the trip. At this location the pressure gradient normalized by the momentum thickness $\delta^{**}$ and the wall shear $\tau_w$ was

$$\frac{\delta^{**}}{\tau_w}\frac{dp}{dx} = 2{\cdot}7 \times 10^{-2}.$$

The mean flow parameters are given in table 1. The friction velocity on the unheated wall was obtained by plotting $\bar{U}/U_\infty$ *vs.* $\log(y/\delta)$ as shown in figure 3 and using the universal constant suggested by Clauser (1956).

The mean and fluctuation levels of the temperature measured by a single wire are shown in figure 4. The skewness and flatness of the temperature are shown in figure 5. The temperature fluctuations have skewness and flatness factors of approximately 0 and 3 respectively in the logarithmic region, which agrees with Zaric (1974) and Fulachier (1972). The large change in these two parameters at $y/\delta > 0{\cdot}5$ indicates the existence of the intermittent region.

### 4.2. *Intermittency and bulge crossing frequency*

Figure 6 shows a typical example of the simultaneous temperature signals from the rake when it is situated in the intermittent region. The locations of the probes are shown to the left of each trace. The non-turbulent fluid is clearly characterized by its quiescent nature and the turbulent bulges are readily apparent in this region. The 'backs' of the bulges, i.e. the portions of the bulges that occur later in time, generally have a temperature gradient $\partial T/\partial x \approx -U^{-1}\,\partial T/\partial t$ that is larger in magnitude than the gradient associated with the fronts. By examination of this and similar data, the strong temperature decrease on the 'backs' was found to be more coherent and penetrated further into the fully turbulent region.

Five different time records of the simultaneous intermittency function $I(\mathbf{x}, t)$ are shown in figure 7. Each record is shown as one strip and has a non-dimensional length of $U_\infty \Delta t/\delta = 4{\cdot}4$. The data points denote where $I(\mathbf{x}, t)$ is 1, and are plotted at successive time steps. In general, the temperature technique indicates that there are not as many non-turbulent holes within the turbulent region nor detached turbulent patches of

| | |
|---|---|
| Free-stream velocity | $U_\infty = 4{\cdot}57$ m/s |
| Boundary-layer thickness | $\delta = y(\overline{U}/U_\infty = 0{\cdot}99) = 9{\cdot}42$ cm |
| Displacement thickness | $\delta^* = \int_0^\infty \left(1-\frac{\overline{U}}{U_\infty}\right) dy = 1{\cdot}34$ cm |
| Momentum thickness | $\delta^{**} = \int_0^\infty \frac{\overline{U}}{U_\infty}\left(1-\frac{\overline{U}}{U_\infty}\right) dy = 0{\cdot}92$ cm |
| Shape factor | $H = \delta^*/\delta^{**} = 1{\cdot}46$ |
| Friction velocity | $u_* = 0{\cdot}041 U_\infty$ |
| Reynolds number | $U_\infty \delta/\nu = 29\,000$ |
| Temperature difference between the wall and the free stream | $T_w - T_\infty = \begin{cases} 11{\cdot}7\,^\circ\text{C} & \text{for rapid cooling measurements} \\ 12{\cdot}8\,^\circ\text{C} & \text{for measurements in the intermittent region} \end{cases}$ |

TABLE 1. Kinematic and thermal parameters.

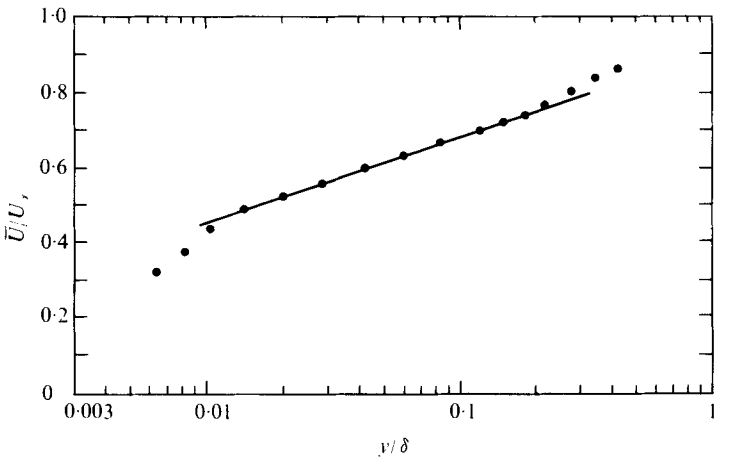


FIGURE 3. Velocity distribution in the turbulent boundary layer without heating.

fluid in the irrotational parts as were reported by Kaplan & Laufer (1969) and Paizis & Schwarz (1974). The remaining isolated regions shown in figure 7 are believed to be due to the three-dimensionality; i.e. they are either turbulent regions connected to bulges at the side or 'eyes' within the turbulent region. The figure clearly shows that the interface position is not a single-valued function. Also the slope of the interface is steeper on the 'fronts' than on the 'backs', which agrees with the results of Kaplan & Laufer (1969) and others.

The intermittency $\gamma(y)$ is the probability that the fluid at that location will be turbulent. Corrsin & Kistler (1955) established that $\gamma(y)$ can be approximated by the complementary error function:

$$\gamma(y) = \tfrac{1}{2}\left[1 - \mathrm{erf}\left(\frac{y-\overline{Y}}{2^{\frac{1}{2}}\sigma}\right)\right], \tag{14}$$

where

$$\mathrm{erf}(x) = \frac{2}{\pi^{\frac{1}{2}}}\int_0^x \exp(-u^2)\, du,$$

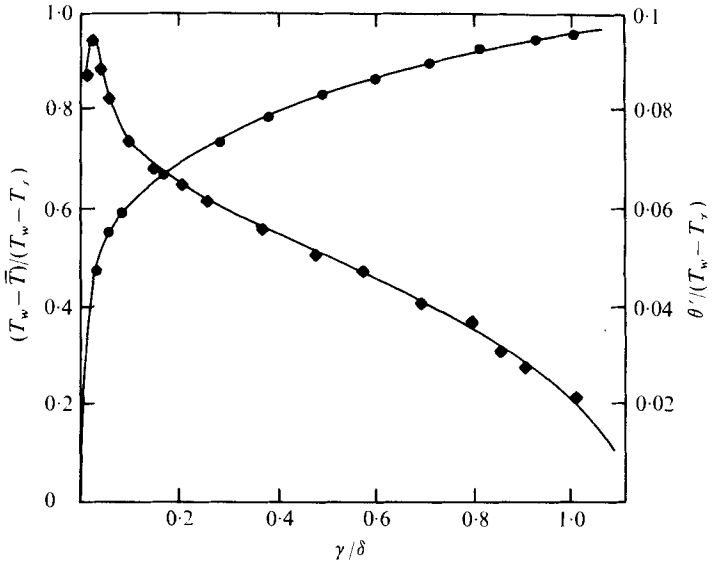


FIGURE 4. Distribution of the mean temperature and the r.m.s. temperature fluctuations: ●, $(T_w-\overline{T})/(T_w-T_\infty)$; ◆, $\theta'/(T_w-T_\infty)$.

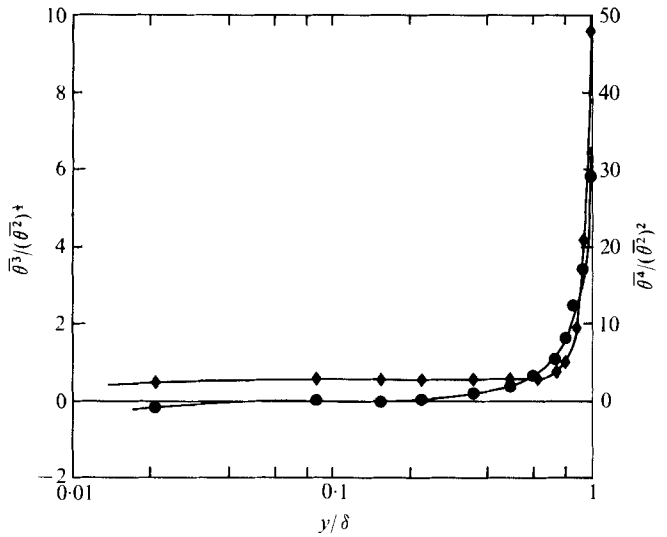


FIGURE 5. Distribution of the temperature skewness and flatness factors: ●, $\overline{\theta^3}/(\overline{\theta^2})^{\frac{3}{2}}$; ◆, $\overline{\theta^4}/(\overline{\theta^2})^2$.

$\overline{Y}$ is the position at which $\gamma = 0{\cdot}5$ and $\sigma$ is the standard deviation of the interface position, which gives a measure of the width of the intermittent region. These two parameters were obtained by plotting the experimental data on Gaussian probability paper and were found to be

$$\overline{Y}/\delta = 0{\cdot}82, \quad \sigma/\delta = 0{\cdot}13, \quad \sigma/\overline{Y} = 0{\cdot}17.$$

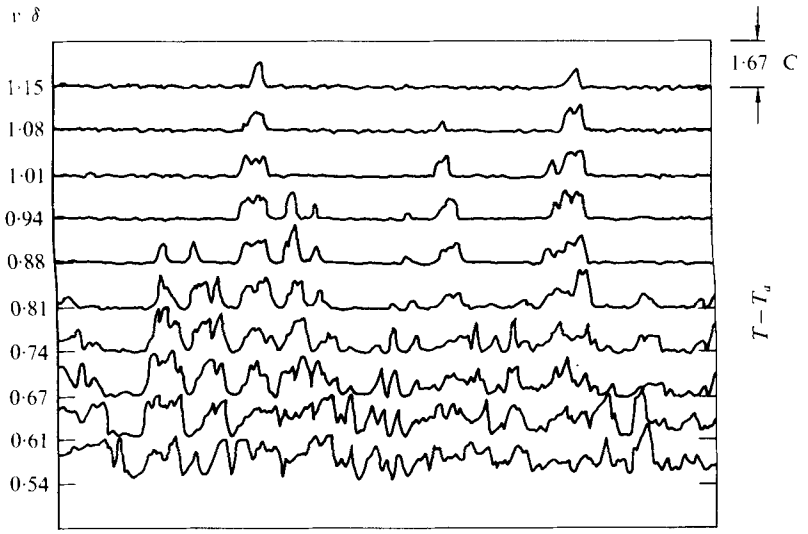


FIGURE 6. Simultaneous temperature signals from the ten-wire rake in the intermittent region. The horizontal time span is $6{\cdot}2\delta/U_\infty$.

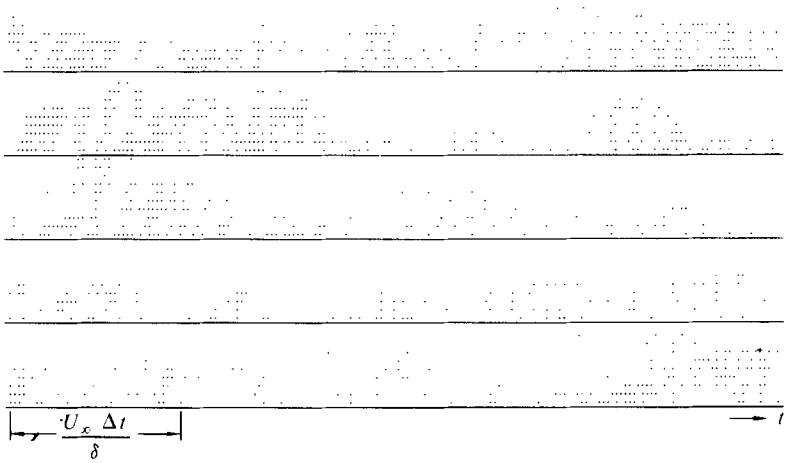


FIGURE 7. Simultaneous records of the intermittency function.

A comparison with the results of other researchers is shown in table 2. Figure 8 shows the experimentally determined intermittency factor. The solid curve in the figure is the complementary error function with the above values of $\overline{Y}$ and $\sigma$.

Thomas (1973) suggested that the bulge crossing frequency $F(y)$, defined as the number of bulges crossing the probe per unit time, was proportional to the exponential function:

$$F(y) \sim \frac{1}{(2\pi)^{\frac{1}{2}}\sigma} \exp\left[-\left(\frac{y-\overline{Y}}{2^{\frac{1}{2}}\sigma}\right)^2\right] = \frac{d\gamma}{dy}. \tag{15}$$

Figure 8 shows this exponential function along with the experimental values of the bulge crossing frequency at each probe location. The constant of proportionality was

| | Chen | Fulachier | Kovasznay *et al.* | Corrsin & Kistler | Hedley & Keffer |
|---|---|---|---|---|---|
| $\sigma/\overline{Y}$ | 0·17 | — | 0·18 | 0 20 | 0·32 |
| $\sigma/\delta$ | 0·13 | 0·14 | 0·14 | 0·16 | 0·24 |
| $\overline{Y}/\delta$ | 0·82 | 0·8 | 0·78 | 0·80 | 0·75 |
| $\sigma/\delta^*$ | 0·91 | — | 0·98 | 0·89 | 2·62 |
| $\overline{Y}/\delta^*$ | 5·77 | — | 5·33 | 4·54 | 8·20 |

TABLE 2. Comparison of mean position and width of the turbulent/non-turbulent interface.

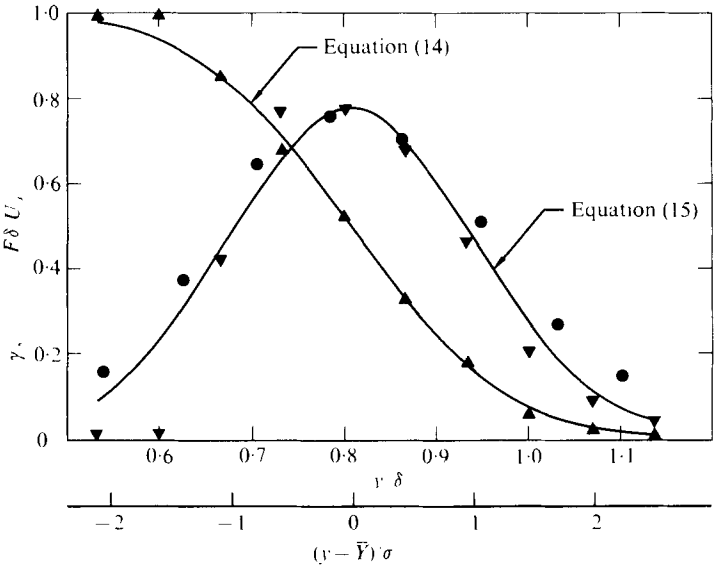


FIGURE 8. The measured intermittency and bulge crossing frequency. ▲, $\gamma$; ▼, $F\delta/U_\infty$; ●, crossing frequencies of Kovasznay *et al.* The curve for the intermittency $\gamma$ is from (14) and that for the bulge crossing frequency $F$ is given by (15).

chosen such that the exponential function had the same value as the experimental data at $\overline{Y}$. The crossing frequency data of Kovasznay *et al.* (1970) are also shown in figure 8. The agreement is quite good except deep in the boundary layer.

### 4.3. *Zone averages of temperature*

The turbulent conditional average $\tilde{\overline{T}}-T_\infty$ and the non-turbulent conditional average $\tilde{\overline{T}}-T_\infty$ together with $\overline{T}$ are plotted *vs.* $y/\delta$ in figure 9. The difference between the turbulent and non-turbulent conditional averages is about 3 % of $T_w-T_\infty$ at $y/\delta = 1{\cdot}15$ and increases towards the wall, reaching a value of 8·3 % of $T_w-T_\infty$ at $y/\delta = 0{\cdot}54$.

It is seen that the non-turbulent zone averages vary across the layer, possibly indicating a stratification in the non-turbulent fluid. This has been observed also by Fulachier (1977, private communication), who has suggested that this effect may be due to thermal conduction. The distance over which heat diffuses in a time $t$ is given by $(tk)^{\frac{1}{2}}$, where $k$ is the thermal diffusivity. Since the boundary layer required roughly 1 s to traverse the tunnel to the test station, the diffusion length scale is approximately

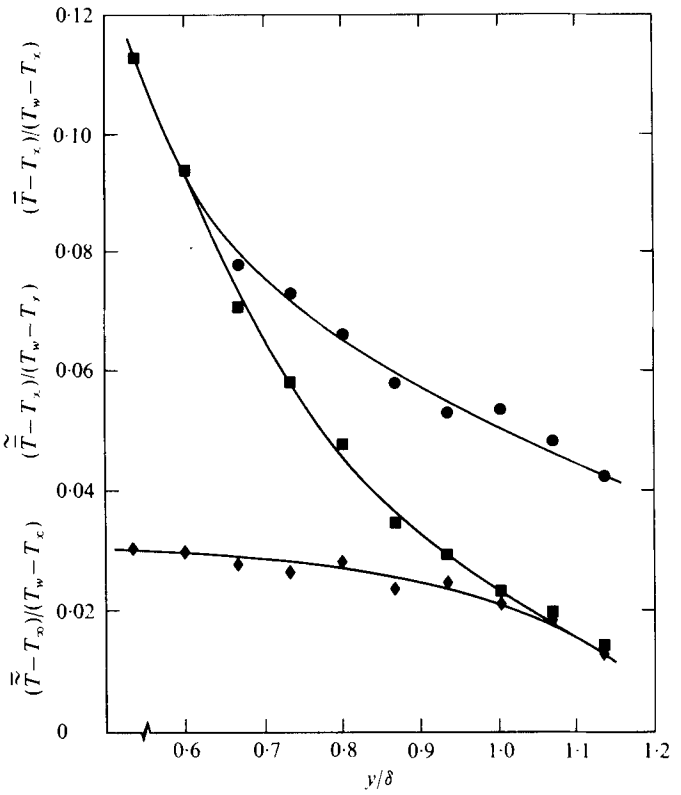


FIGURE 9. The turbulent zone average, the non-turbulent zone average and the conventional average of the temperature: ●, $(\bar{\tilde{T}}-T_\infty)/(T_w-T_\infty)$; ◆, $(\tilde{\bar{T}}-T_\infty)/(T_w-T_\infty)$; ■, $(\bar{T}-T_\infty)/(T_w-T_\infty)$.

0·5 cm. Although this is much smaller than the distance between the bulges, it is of the same order of magnitude as the experimentally observed thickness of the interface. Since the Prandtl number is approximately unity in air, the same argument is valid for the vorticity diffusion. This possibly explains why the interface is normally observed to be considerably thicker than the Kolmogorov microscale, as was originally proposed by Corrsin & Kistler (1955). On the other hand, the variation of $\tilde{T}$ may be due to heat conduction to and from the prongs of the temperature probes as they enter and leave the warmer turbulent bulges.

Figure 10 shows the r.m.s. fluctuation level of the temperature for each separate zone. This is achieved by sampling the mean-square fluctuation about the conditionally averaged mean temperature. The instantaneous fluctuation around the conditionally averaged mean temperature is defined as $\theta_T(t) = T(t) - \bar{\tilde{T}}$ in the turbulent zone and $\theta_N(t) = T(t) - \tilde{\bar{T}}$ in the non-turbulent zone, so that $\bar{\theta}_T = \bar{\theta}_N = 0$. Then the corresponding r.m.s. values are $\bar{\tilde{\theta}}' = (\bar{\tilde{\theta}}_T^2)^{\frac{1}{2}}$ and $\tilde{\bar{\theta}}' = (\tilde{\bar{\theta}}_N^2)^{\frac{1}{2}}$. The conventional r.m.s. value is denoted by $\theta'$. The relation between $\theta'$, $\tilde{\theta}'$ and $\bar{\theta}'$ can be derived and is

$$\bar{T}^2 + \theta'^2 = \gamma\{\bar{\tilde{T}}^2 + \bar{\tilde{\theta}}'^2\} + (1-\gamma)\{\tilde{\bar{T}}^2 + (\tilde{\bar{\theta}}')^2\},\dagger \tag{16}$$

† This equation was derived first by Kovasznay *et al.* and corrected by Paizis & Schwarz (1975) for velocity. Both derivations were erroneous. Equation (16) is equivalent to the equation used by Hedley & Keffer (1974*b*).

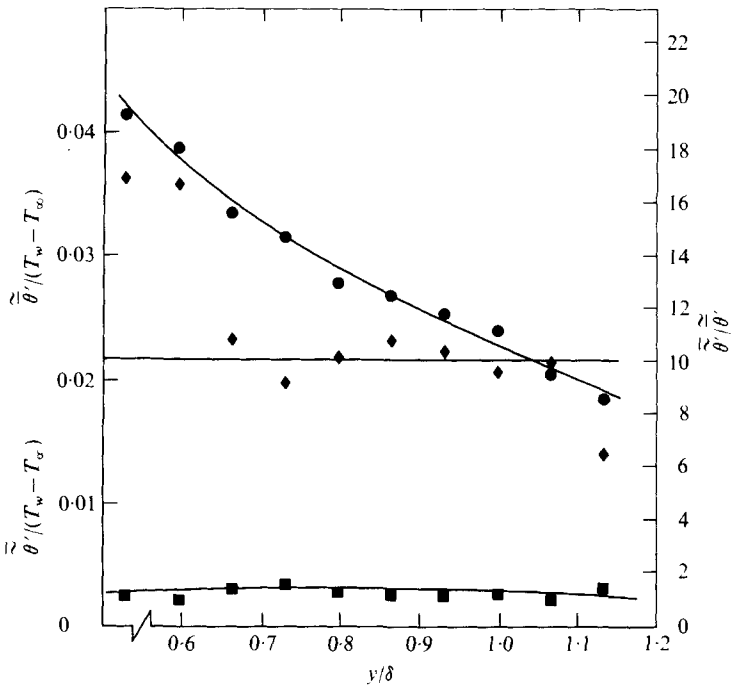


FIGURE 10. Zone average of the turbulent r.m.s. fluctuations, zone average of the non-turbulent r.m.s. fluctuations and their ratio: ●, $\overline{\tilde{\theta}'}/(T_w - T_\infty)$; ■, $\overline{\tilde{\theta}'}/(T_w - T_\infty)$; ◆, $\overline{\tilde{\theta}'}/\overline{\tilde{\theta}'}$.

which was experimentally verified for all the data. In the non-turbulent region, the fluctuations were approximately constant and equal to 0·04 °C. In the turbulent zones, the fluctuations were roughly an order of magnitude greater and increased in magnitude closer to the wall. The ratio $\overline{\tilde{\theta}'}/\overline{\tilde{\theta}'}$ is also shown in figure 10. It has a value of 10 or larger everywhere except in the extreme outer region. At $y/\delta = 1{\cdot}15$, it decreases to 6 and is expected to decrease further as $y$ increases since the turbulent fluctuation within the bulge is seen to decrease faster than the fluctuation level in the ambient fluid.

The effectiveness of a detection function depends on the contrast between the signals in the two zones as discussed in the appendix. The signal-to-noise ratio for the interface detection can be defined as the ratio of the fluctuation level of the detection signal in the turbulent zone to that in the non-turbulent zone. In the present study, $\overline{\tilde{\theta}'}/\overline{\tilde{\theta}'}$ is approximately 10 throughout the intermittent region. Kovasznay *et al.* (1970) found that, because of the irrotational velocity fluctuations outside the boundary layer, their signal-to-noise value varied from approximately 4 for $y/\delta < 0{\cdot}9$ to 9·7 for $y/\delta \approx 1{\cdot}1$. This indicates that it is easier to formulate a detection function based upon the temperature signal than one based upon $\partial^2 u/\partial y\,\partial t$, throughout most of the intermittent region.

### 4.4. *Point averages of temperature*

The distributions of point averages of temperature for the 'fronts' and 'backs' are shown in figure 11. The detector probe was chosen to be one sensor from the rake and the other probes were sampled simultaneously whenever an interface crossed the detector location. Data were analysed for five different detector positions which were

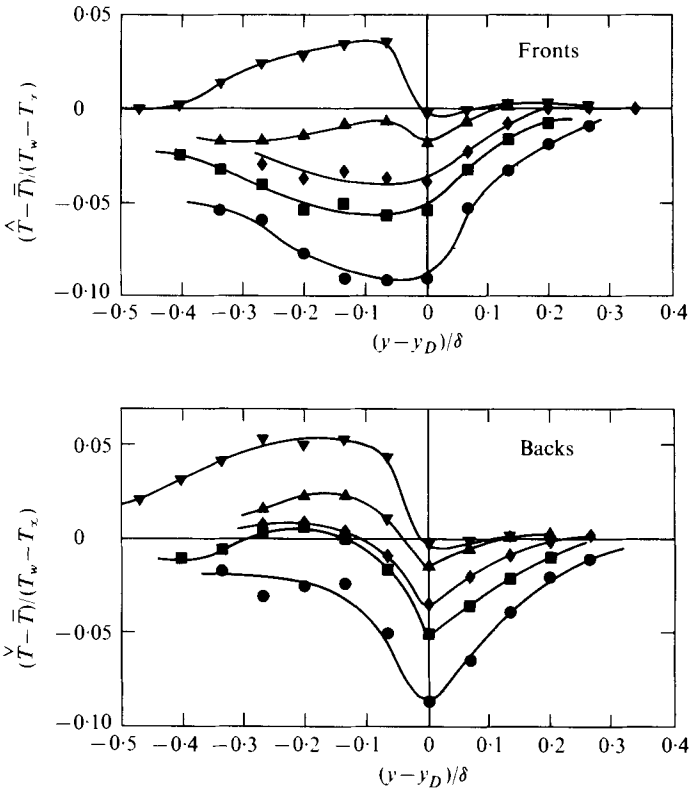


FIGURE 11. Point averages of temperature as a function of the distance from the interface; $T_w - T_\infty = 12{\cdot}8\,^\circ\mathrm{C}$. $\gamma(y_D)$: ●, 0·84; ■, 0·65; ◆, 0·56; ▲, 0·37; ▼, 0·18.

characterized by the corresponding values of the intermittency factor:

$$\gamma(y_D) = 0{\cdot}18, 0{\cdot}37, 0{\cdot}56, 0{\cdot}65, 0{\cdot}84.$$

Data were taken with the rake at two different and overlapping locations in order to check the statistical repeatability and to provide sufficient resolution beneath the interface. Each curve gives the ensemble average of the difference between the sampled temperature at the time at which the interface crossed the detector probe and the local mean value of the temperature. Since the interface position is multi-valued, as seen in figure 7, the point averages in figure 11 contain data from both the turbulent and the non-turbulent regions.

Away from the interface the point averages all converge to zero as they must. For $\gamma = 0{\cdot}18$, the point averages are higher than the mean temperature beneath the interface, i.e. $y < y_D$, the 'backs' being warmer than the 'fronts'. When $\gamma > 0{\cdot}18$, the point averages beneath the interfaces on the 'fronts' and the 'backs' are quite different. On the fronts, the point averages $\hat{T} - \overline{T}$ are always negative and approximately constant for the first $0{\cdot}2\delta$ inside the interface, whereas the point averages $\check{T} - \overline{T}$ on the backs have an abrupt change in slope at the interface and approach zero deeper in the layer.

Temperature measurements alone cannot reveal the large-scale motion in the intermittent region. However, when these measurements are considered with the point averages of the streamwise and normal velocity components obtained by Kovasznay

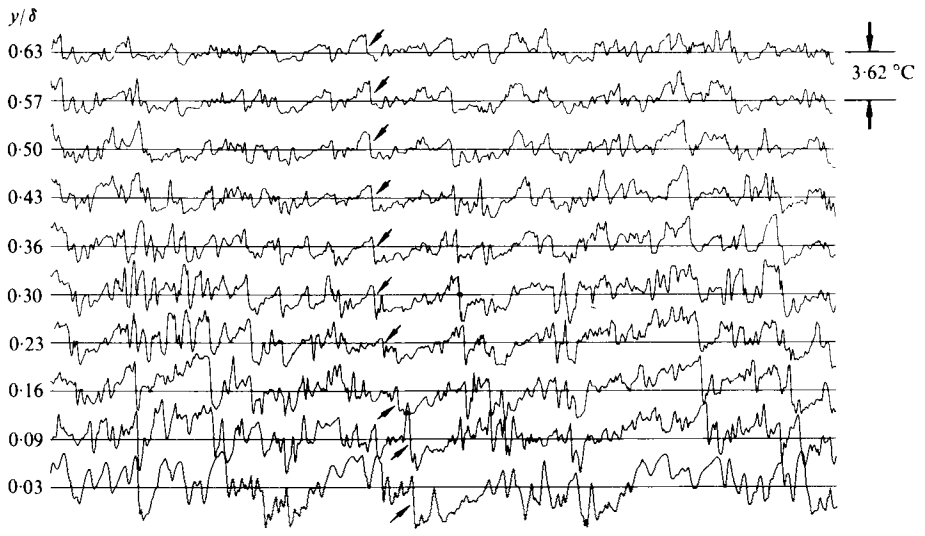


FIGURE 12. Simultaneous temperature signals from the ten-wire rake in the turbulent region. The horizontal time span is $18{\cdot}7U_\infty \Delta t/\delta$. One particular temperature front is denoted by the arrows.

*et al.* (1970) and Blackwelder & Kovasznay (1972), a clearer picture of the flow field seems to emerge. For $\gamma < 0{\cdot}3$ and relative to the local mean velocity and temperature field, warm fluid with a streamwise momentum deficit is moving upwards near the 'backs' and downwards near the 'fronts' inside the interface. For $\gamma > 0{\cdot}7$ cool fluid with a streamwise momentum excess is moving into the turbulent region in the valleys of the interface and riding over the turbulent bulge otherwise.

### 4.5. *Internal temperature fronts*

The most interesting result of this investigation was the observation of large-scale temperature fronts that often extended over the entire boundary layer. Several examples of these fronts can be seen in figure 12, which displays the simultaneous temperature traces for $0{\cdot}03 \leqslant y/\delta \leqslant 0{\cdot}63$. Thus the outermost trace is in the intermittent region and the lowermost trace is in the wall region ($y = 0{\cdot}03\delta$ corresponds to $y^+ = 35$). Usually a particular temperature front was not observed at all ten probe locations. This was expected because the probes can obtain only a quasi-two-dimensional sample from the front, which is presumably a three-dimensional structure. Figure 12 does however show some temperature fronts which seem to span the entire distance covered by the probes.

It is readily seen that the temperature front is skewed in the $y$ direction. This is characterized by a definite time delay between the front passage at any two different probe locations. The temperature fronts were always associated with strong temperature decreases. This is what provides the striking visual correlation in figure 12. Although a few sharp temperature increases can be observed locally, they are not correlated in the normal direction and hence seem to be only random statistical fluctuations unassociated with any structure. Also the structure characterized by the temperature front is not associated with any particular part of the boundary layer, but occurs at all locations. Indeed, this is one of its most significant properties because

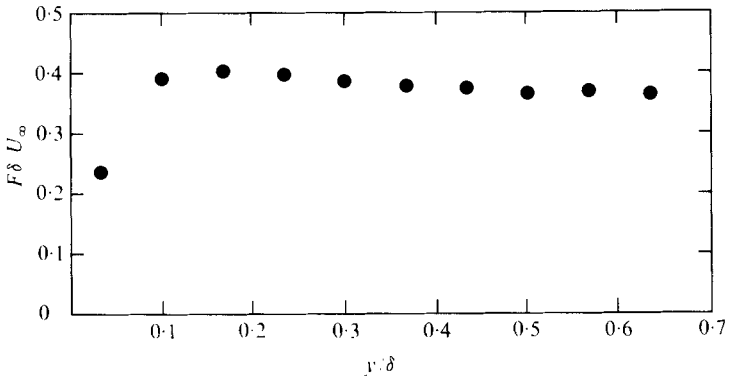


FIGURE 13. Frequency of detection of the internal temperature front.

it seems to provide a dynamical relationship between the large-scale structure in the intermittent region and the eddy structure near the wall, as will be discussed later.

### 4.6. *Crossing frequency of the temperature fronts*

The detection of the internal temperature fronts was accomplished by using the technique described in § 3.2. Figure 13 shows the average number of temperature fronts that crossed the detector probe per unit time normalized with the outer variables $U_\infty$ and $\delta$. Since figure 12 and similar data indicated that not all the internal temperature fronts extended across the fully turbulent region, it is somewhat surprising to see that $F\delta/U_\infty$ has essentially a constant value of 0·38 over the entire region. These values are quite similar to the average crossing rate of the interface in the intermittent region as shown in figure 8. Examination of the simultaneous data, such as those shown in figures 6 and 12, indicated that whenever a cold temperature front appeared in the upper fully turbulent region it often extended into the intermittent region and coincided with one of the 'backs'. However, not all of the 'backs' could be associated with a strong temperature front that extended into the fully turbulent region. This may be due to the three-dimensional nature of the structure as explained earlier. The inverse of the crossing frequency gives the average time between the temperature fronts. When multiplied by $U_\infty$, the average distance between the fronts is approximately three boundary-layer thicknesses.

### 4.7. *Coincident correlation measurements*

The coincident correlation technique and Taylor's hypothesis were used to determine the most probable shape of the internal temperature in the $x, y$ plane. This was accomplished by finding the average phase lag of the fronts between the relative locations of the probes. Examination of the simultaneous temperature traces indicated that the front almost always crossed the outermost position first. The coincident correlation coefficients were computed using (13) and some typical results are shown in figure 14. The time delay corresponding to the maximum correlation represents the most probable phase lag between the front crossing at $y_0$ and its neighbour at $y_0 - \Delta y$. As can be seen, it is positive and varies from $U_\infty \tau/\delta = 0{\cdot}025$ in the outer region to approximately 0·2 near the wall.

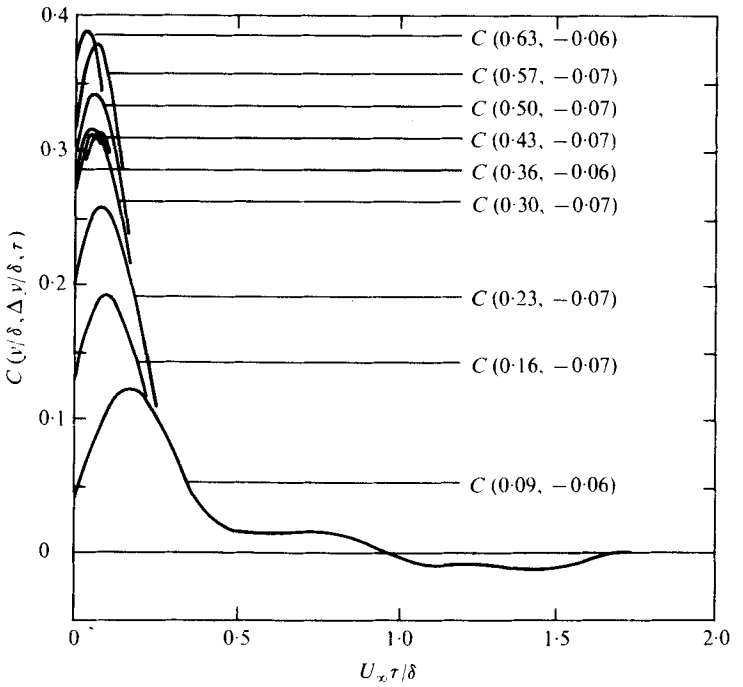


FIGURE 14. Coincidence correlation coefficients obtained from adjacent probes.

Although the lengths of the pulses were always the same and their mean frequency was approximately constant, the shapes of the coincident correlation curves vary considerably, i.e. the maximum decreases and the curves become broader as the wall is approached. By comparison, one can show that, if the fronts extended across the entire boundary layer and had a constant convection velocity and shape in the $x, y$ plane, then the correlations would all be triangular-shaped functions with a maximum normalized magnitude of unity and the time delay at the maximum would be proportional to the local angle of the front. Figure 12 shows that the temperature fronts do not extend across the entire boundary layer as they cross the rake of probes. This effect by itself would not account for the variation in the shape of the normalized correlations shown in figure 14. However, the simultaneous data also show that at any two fixed $y$ locations the temperature fronts did not cross the inner probe at a constant time delay after crossing the outer probe. Thus the shape of the front is not constant and this effect adds a random phase lag between the two positions as discussed by Blackwelder (1977). This decreases the maximum value of the correlation curves and broadens them. Figure 14 indicates that this effect is stronger in the fully turbulent region near the wall, as one would expect because the fluctuations are stronger there, and milder in the outer, intermittent regions.

The accumulated phase lag across the boundary layer with respect to the probe at $y/\delta = 0{\cdot}63$ is shown in figure 15. This curve was obtained by using the coincident correlations between adjacent probe locations and also the most probable phase lag corresponding to the maximum of each curve. The cumulative phase lag at each position was found by summing all the individual lags between $y/\delta = 0{\cdot}63$ and the position of interest. In principle, one would prefer to obtain directly the coincident

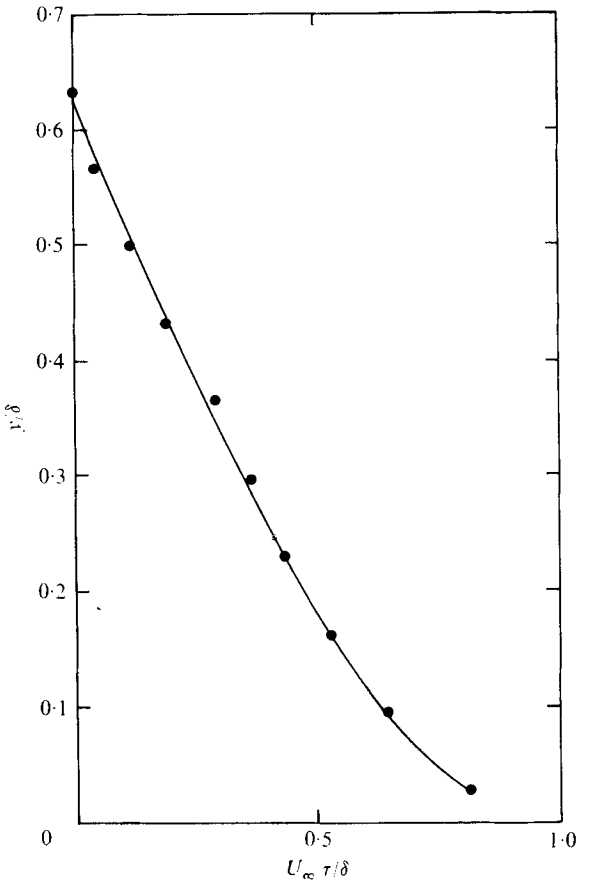


FIGURE 15. The most probable time delay of the temperature front crossing relative to its crossing at $y/\delta = 0{\cdot}63$.

correlation between the signal at $y/\delta = 0{\cdot}63$ and the other positions and use the maximum. In practice, the random phase lag was so great that no well-defined peaks could be established at large spatial separations, i.e. $|\Delta y/\delta| > 0{\cdot}27$. Some correlations were computed directly between locations with $|\Delta y/\delta| > 0{\cdot}06$. The result agreed well with the data in figure 15 and helped to verify the technique. In view of the velocity gradient across the boundary layer, a direct comparison cannot be made between the temporal and spatial shapes of the front. However the curve in figure 15 can be considered as a qualitative description of the mean shape of the temperature front as seen by an observer riding at $y/\delta = 0{\cdot}63$. In this frame of reference, the front extends over approximately one boundary-layer thickness in the upstream direction.

### 4.8. *Simultaneous temperature and velocity measurements*

The triple probe was capable of measuring the temperature and two velocity components and was used to study the motion about the internal front. The conventional transport coefficients between $u$, $v$ and $\theta$, defined as $R_{uv} = \overline{uv}/u'v'$, $R_{u\theta} = \overline{u\theta}/u'\theta'$ and $R_{v\theta} = \overline{v\theta}/v'\theta'$, are shown in figure 16. As reported by Johnson (1959) and Fulachier

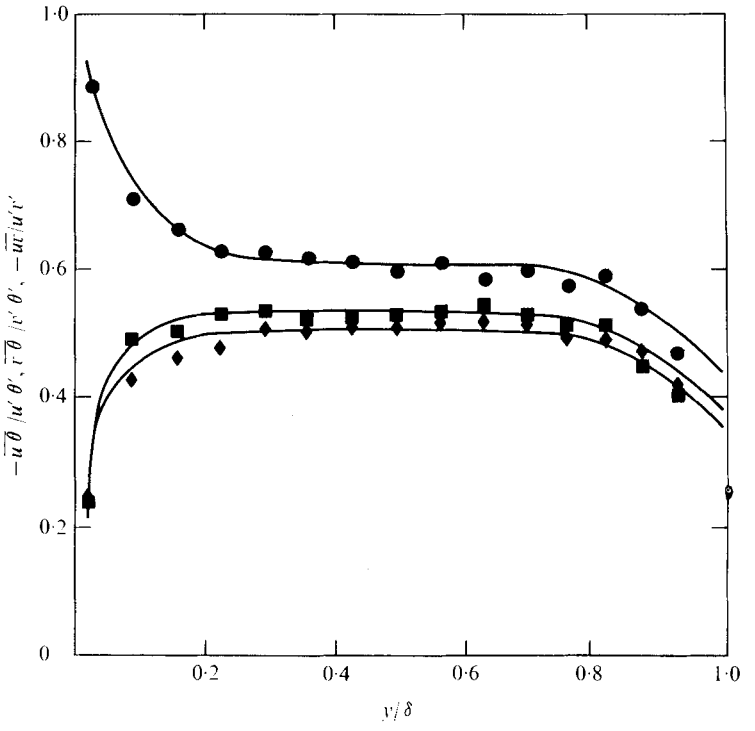


FIGURE 16. Distribution of the turbulent transport coefficients: ●, $(-\overline{u\theta})/u'\theta'$; ■, $(-\overline{uv})/u'v'$; ◆, $(\overline{v\theta})/v'\theta'$.

(1972), $R_{u\theta}$ is very large and strongly negative near the wall, which is indicative of the strong coupling between the streamwise velocity and the temperature fluctuations. Together with the negative values of the skewness of temperature, this suggests that the wall region is constantly disturbed by cold fluid with a high streamwise velocity. The transport coefficients are fairly constant in the interval $0{\cdot}2 < y/\delta < 0{\cdot}7$ and are within 20% of Fulachier's (1972) results. Outside this region the coefficients follow the same trend as was reported by Fulachier.

Figure 17 shows the conditional averages of $\theta$, $u$ and $v$ associated with the internal temperature front. All the data are normalized by the local r.m.s. level. It was found that the normalized time derivative of the conditionally averaged temperature was constant for all the curves and was

$$\left| \frac{\delta}{U_\infty \theta'} \frac{d\langle\theta\rangle}{dt} \right| = 22.$$

However, the fluctuation level of temperature at $y/\delta = 0{\cdot}03$ was 2·4 times as large as that at $y/\delta = 0{\cdot}63$, indicating that the temperature gradient steepens across the front as the wall is approached. If the temporal locations of the negative and positive peaks of the conditionally averaged temperature are used to define the width of the temperature front, it is readily seen that its passage time is approximately constant and is $0{\cdot}1\delta/U_\infty$ across the layer. If the front is convected with the local mean velocity, its corresponding width in the streamwise direction varies from $0{\cdot}05\delta$ to $0{\cdot}1\delta$. Both $\langle u\rangle$ and $\langle v\rangle$ change sign everywhere across the internal front, which indicates that the

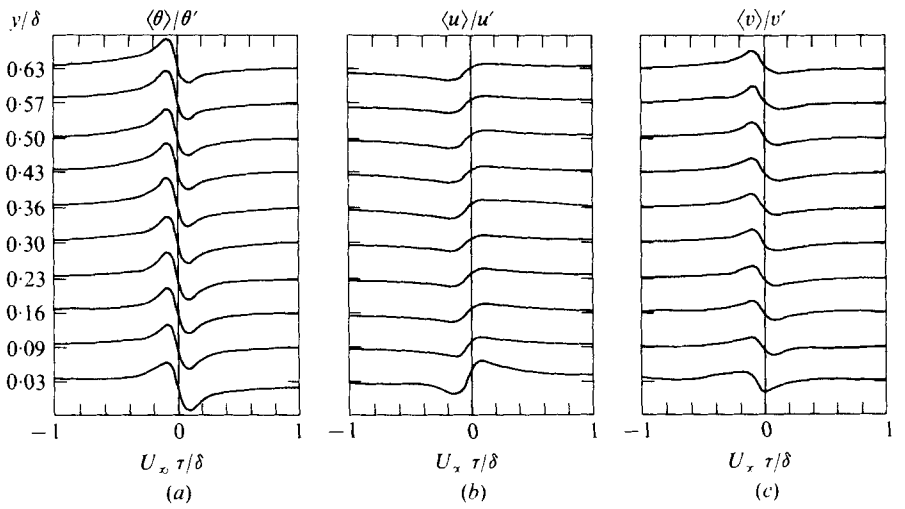


FIGURE 17. Distribution of the conditionally averaged quantities: (*a*) temperature, (*b*) streamwise velocity and (*c*) normal velocity. Each curve represents the time history of the conditional averages referred to the local time of crossing of the internal temperature front. The displacement between the curves is always twice the local r.m.s. value.

temperature front has a deterministic velocity. A negative $\langle u \rangle$ and positive $\langle v \rangle$ are found downstream of the front.

The above results suggest that the temperature front is associated with an internal shear layer that also extends across the boundary layer. The conditional averages show that in general the warmer fluid downstream of the front is associated with low streamwise momentum and is moving away from the wall. Upstream of the front, cooler fluid with higher streamwise momentum is moving towards the wall. Compared with the local fluctuation levels, the relative strength of these two counteracting motions varies across the layer. In the outer intermittent region the conditional averages of figure 17 show that the outward movement on the downstream side of the front is stronger. This motion is associated with the turbulent core of the bulges directly inside the back interface and thus is a reflexion of the fact that there is more coherent motion inside the bulge than there is in the non-turbulent regions.

As the wall is approached, the results in figure 17 cannot be interpreted so easily. It can be seen that the zero crossings of the conditional averages of $u$ and $v$ advance forwards in time relative to the zero crossings of the temperature. Since this difference is very important in analysing the associated turbulent eddy structure, its validity was thoroughly checked for errors. The temperature sensor and the X-probe used to measure the velocity components have a small spatial separation. However, since the temperature sensor was upstream of the X-probe, the resulting phase shift would be in the opposite direction of that observed in figure 17. The effect of the temperature contamination on the velocity probes was carefully studied and it was concluded that it could not be responsible for the observed phase shift. No other errors were found that could explain the observed phase differences and since the results were repeatable, they were accepted as presented.

This indicates that the flow field in the wall region is more complicated than that

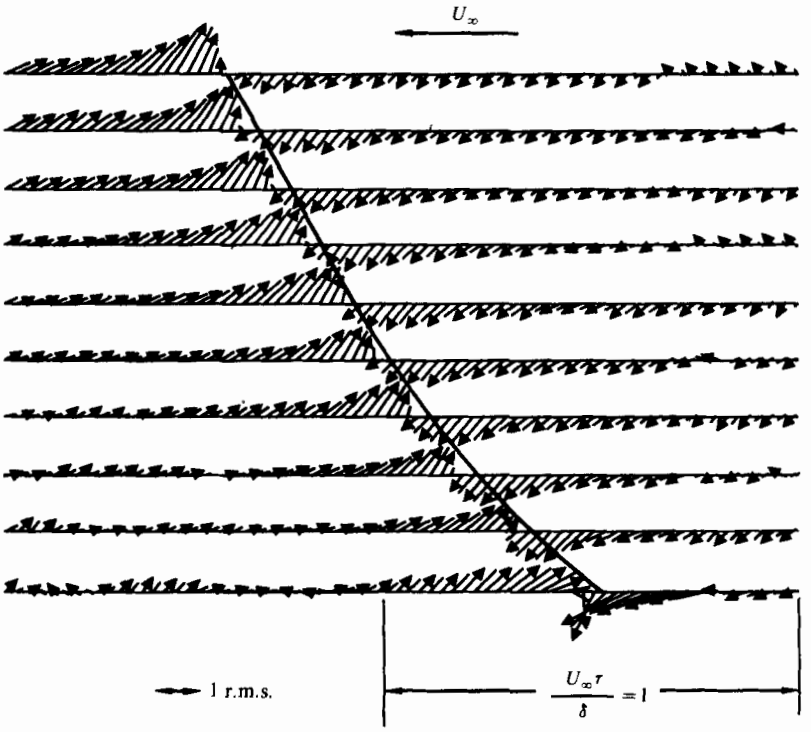


FIGURE 18. Composite picture of the velocity field associated with the internal front. The velocity components are normalized with their local fluctuation levels. The velocity magnitude and time scale are given at the bottom of the figure. For clarity only every other velocity vector has an arrowhead.

further out. For example, these results may indicate that the shear layer and temperature front are not coincident. A more probable explanation is that there is another type of eddy structure associated with the temperature front in the lower region of the boundary layer such as the streamwise vortices described by Kim *et al.* (1971). Since only two velocity components were measured, the motion associated with the third velocity component may be responsible for the phase shift.

A composite picture of the two-dimensional velocity field associated with the temperature front is shown in figure 18. This figure uses the mean location of the temperature front found in figure 15. Then the velocity data of figure 17 are replotted using the position of the front as the reference time at each $y$ position. The local mean values of the two velocity components have been subtracted and the difference plotted as a vector with a magnitude and direction. Thus at each normal position the relative velocity is shown for time delays before and after the crossing of the temperature front. Directly before the internal front, there is an outward motion of warmer fluid away from the wall. After the front has passed, the cooler fluid with an excess of streamwise momentum is seen moving towards the wall. The phase difference between the zero crossings of the temperature and momentum is clearly evident near the wall. It seems that there are small temporal zones in which warm high speed fluid is moving towards the wall, although such a strict Lagrangian interpretation of the present data is not possible.

## 5. Discussion and conclusions

The use of a small amount of heat as a passive contaminant was found to be a very valuable technique for studying the large-scale motion in the turbulent boundary layer. By uniformly heating the boundary layer from its beginning, the heat served as a tracer for the turbulence. With low heat flux, the dynamical structures in the shear layer were virtually unchanged. Thus in the outer, intermittent regions the temperature signals were accurately able to identify the turbulent/non-turbulent interface. The conditional averages of the temperature and velocities in this region readily verified the motion described by Kaplan & Laufer (1969), Kovasznay *et al.* (1970), and others.

The predominant structure illustrated by the heat contamination was the sharp internal temperature front that existed throughout all regions of the flow field. This temperature front was characterized by a rapid temporal change from warmer to cooler fluid. In the outer, intermittent region, the fronts were readily associated with the backs of the bulges, such that the warmer fluid was inside the bulges and the cooler fluid was associated with the non-turbulent region between the bulges. The strongest temperature changes in time were always associated with the backs. The point averages also showed sharper spatial gradients near the backs and rather homogeneous temperatures below the fronts. Hedley & Keffer (1974*b*) found also that the strongest changes in the point averages of the Reynolds stress were near the backs. Thus the structure associated with the backs seems to be more dynamical while the fluid near the fronts is more homogeneous and better mixed. This supports a model proposed by Kovasznay (1970) in which a parcel of fluid of low streamwise momentum moves into the intermittent region from below. The 'back' of the bulge coincides with this fluid parcel. The 'front' is the boundary of the wake formed by the high speed irrotational fluid moving around it.

The simultaneous temperature signals showed that the temperature fronts extended down into the fully turbulent region as clearly identifiable structures. The fronts were highly three-dimensional, and thus a single front only rarely passed over the entire rake of sensors, which formed a straight line perpendicular to the wall. However, the conditional averages associated with the front were similar across the entire boundary layer and the mean frequency of occurrence was approximately constant everywhere. Whenever a sharp temperature decrease occurred at one spatial location, one could also observe it at two or more neighbouring locations with a slight time shift. Thus it was felt that this structure usually extended across the entire boundary layer. However since it was of finite width in the spanwise direction, part of it was out of the plane of the sensors.

The streamwise and normal velocity components also experienced very sharp and rapid changes in the vicinity of the temperature front. Although the magnitudes of the velocity changes normalized by the local r.m.s. values were usually not as large as the temperature change, they do suggest that an internal shear layer was associated with the temperature front. In the outer, intermittent region, both the temperature front and the shear layer were clearly associated with the backs of the turbulent bulges. As the wall was approached, the conditional averages of velocity and temperature indicated that the front and the shear layer were not coincident in time, as seen in figure 18. This was manifested by a phase shift between the zero crossings of the averaged velocity and temperature signals. This phase shift may have been due to

some aspect of the eddy structure that was not measurable with the available probes and experimental configurations, e.g. streamwise vortices.

In the present study, the location closest to the wall was $y/\delta = 0{\cdot}03$, which corresponded to $y^+ = 35$. Both the detection of the temperature front and the sampling of the data occurred there. Blackwelder & Kaplan (1976) detected the bursting phenomenon at $y^+ = 15$ and then sampled data at positions throughout the wall region. The ensemble averages found in figure 17 are very similar to those reported by Blackwelder & Kaplan; i.e. a sequence of regions of low streamwise momentum moving away from the wall followed by a very sharp streamwise acceleration and high velocity fluid moving towards the wall. Furthermore, this sequence shown in figures 17 and 18 has also been found by Wallace, Brodkey & Eckelmann (1977) at several points in space extending from $y^+ = 3{\cdot}4$ to $y^+ = 195$. Although they did not make simultaneous measurements at more than one point in space, their results suggest that a structure similar to the temperature front occurs throughout the entire layer. In addition, the detection scheme of Blackwelder & Kaplan was applied to the velocity data at $y^+ = 35$. The conditional averages were quite similar to those at $y/\delta = 0{\cdot}03$ in figure 17, which again strongly suggests that the bursting phenomenon is indeed closely related to the temperature front. Also supporting this relationship is the fact that the frequency of occurrence of the temperature front in figure 13 is approximately the same as the mean frequency of the bursts reported by Rao *et al.* (1971), Laufer & Badri Narayanan (1971) and others.

The internal shear layer separates a region of relatively low speed fluid downstream from the high speed fluid on the upstream side. Thus it may well represent the demarcation line between the accelerated and decelerated fluid regions observed by Nychas *et al.* (1973). They found that these two regions were often in close proximity; however they were not able to observe a sharp and distinct interface between the two regions. This may possibly have been due to their visualization technique or to their convected frame of reference. Below $y^+ = 70$, their observed interface was sharper and the incoming high speed fluid interacted with the ejected fluid associated with the bursting phenomenon near the wall. They reported that the burst occurred first and then moved into the oncoming accelerated region. This may be related to the conditional averages in figures 17 and 18, which show that the velocity signals associated with the bursting phenomenon occurred slightly earlier than the internal temperature front.

The internal shear layer is definitely important in the transport processes in the turbulent boundary layer as can be seen from its relationship to the temperature front. The evidence also suggests that it provides a possible mechanism by which the large-scale structure in the outer, intermittent region is related to the bursting phenomenon near the wall. A physical mechanism linking these two structures has been suggested by several authors, as discussed in the review articles by Kovasznay (1970), Laufer (1975) and Willmarth (1975). Although the present data are not conclusive, they do indicate that the internal shear layer does tie these two eddy structures together in a deterministic manner and hence is of considerable importance in the dynamics of the turbulent boundary layer.

The authors wish to express their appreciation to Professor John Laufer, who originally helped to formulate this research. Both he and Professor Richard E. Kaplan made many useful suggestions and criticisms during the course of this work. Mr Tim Jentes was very helpful in the design and construction of the constant-current resistance thermometers. This research was jointly supported by the National Science Foundation under grant GK-35800X and the Office of Army Research under grant DA-ARO-D-31-124-73-G118. Their support is gratefully acknowledged.

## Appendix

In order to study the intermittent region of free turbulent shear flows, it is highly desirable to be able to separate the flow field into two classes; one being characterized by turbulence and the other by the lack of it. With such a separation, the two classes can be studied independently and consequently better models of the interface and intermittent region can be constructed. This is especially desirable when one attempts to model the entrainment of non-turbulent fluid into the vortical regions.

The separation process is usually accomplished by a detection scheme based upon some signal $Q(t)$ derived in the intermittent region of the shear flow. The results of the detection process crucially depend upon the initial choice of $Q(t)$. It is difficult to prescribe rigid rules for choosing $Q$. However some guidelines can be formulated by examining the probability density of $Q$, which may be written as

$$p(Q) = (1-\gamma)\,p^n(Q) + \gamma p^t(Q), \tag{A 1}$$

where $\gamma$ is the intermittency factor and $p^n(Q)$ and $p^t(Q)$ are the probability densities of $Q$ in the non-turbulent and turbulent classes. These probability densities are plotted schematically in figure 19. If $\tilde{Q}$ and $\bar{\tilde{Q}}$ are the average values of $Q$ in the turbulent and non-turbulent zones respectively, then it is apparent that the inter-class distance, represented by the difference between $\tilde{Q}$ and $\bar{\tilde{Q}}$ should be as large as possible, as pointed out by Hedley & Keffer (1974*a*). An additional criterion is that the intra-class distance should be as small as possible; i.e. the width of the probability density of each class as measured by its r.m.s. value, for example, should be small.

Such signals are rarely found in nature. Hence the usual laboratory technique is to choose a signal $Q_1(t)$ initially and then process it by a circuit or algorithm that is often nonlinear to derive a signal $Q_2(t)$. The properties of $Q_2(t)$ are then tested by some criteria to determine if it is suitable for detecting the two different classes. If it is not, further iteration is performed until an acceptable signal is derived.

Obviously one desires to choose initially a signal whose features have the greatest contrast between the two classes. Since turbulence is defined as that fluid which possesses three-dimensional random vorticity, the rectified vorticity signals, or some combination thereof, would be a likely candidate for the signal $Q(t)$. Kibens, Kovasznay & Oswald (1974) used a vorticity meter sensitive to the streamwise vorticity in order to form a detection scheme. Since a vortiticy meter is difficult to construct, other authors have used more simply derived signals. Examples include the use of the streamwise velocity component by Kaplan & Laufer (1969), Paizis & Schwarz (1974) and others, the use of $\partial^2 u/\partial y\,\partial t$ by Kovasznay *et al.* (1970), the use of a combination of the time derivatives of $u$ and $v$ by Hedley & Keffer (1974*b*), etc.

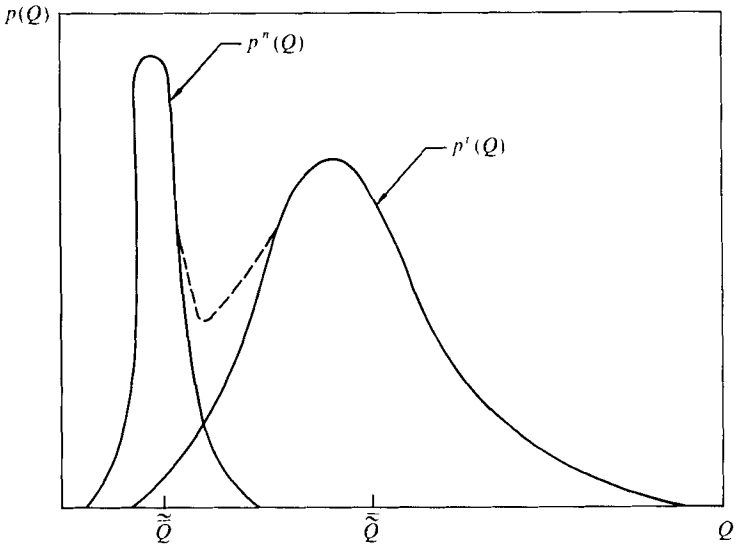


FIGURE 19. Probability densities of $Q$ in the turbulent and non-turbulent regions.

Several recent investigations, including this one, have used a temperature signal for $Q(t)$; examples include the work by LaRue & Libby (1974), Kovasznay & Ali (1974) and Antonia, Prabhu & Stephenson (1975). This technique is popular because it provides a relatively large inter-class distance; i.e. the turbulent fluid is hot and the non-turbulent fluid is cold or vice versa. Thus it often eliminates the need for additional processing of the signal.

All of the previously used signals and techniques involve some subjectivity in designing the filtering function, choosing a threshold value, etc. However by using the underlying probability densities associated with $Q(t)$, a more objective technique can be developed. Bilger, Antonia & Sreenivasan (1976) used this technique to determine the intermittency factor. The present analysis was developed in order also to determine the conditional averages and the crossing frequency.

Using the probability distribution given by (A 1), one can easily define the average values in the turbulent and non-turbulent zones or classes as

$$\tilde{\tilde{Q}} = \int_{-\infty}^{\infty} Q p^n(Q)\, dQ, \tag{A 2}$$

$$\bar{\tilde{Q}} = \int_{-\infty}^{\infty} Q p^t(Q)\, dQ. \tag{A 3}$$

Hence the first moment of (A 1) yields

$$\bar{Q} = (1-\gamma)\tilde{\tilde{Q}} + \gamma \bar{\tilde{Q}}. \tag{A 4}$$

Experimentally one defines an intermittency function as

$$I(Q_d, t) = \begin{cases} 1 & \text{if } Q > Q_d, \\ 0 & \text{otherwise,} \end{cases} \tag{A 5}$$

where $Q_d$ is the threshold value. The estimated value $\gamma_e$ of the intermittency factor is defined as the probability that $Q$ is greater than the threshold. Hence

$$\gamma_e(Q_d) = \Pr\{Q > Q_d\} = \int_{Q_d}^{\infty} p(Q)\,dQ. \tag{A 6}$$

Similarly the estimated value $\tilde{\bar{Q}}_e$ of the conditional average in the turbulent region is the conditional probability of $Q$ given that $Q > Q_d$, i.e.

$$\tilde{\bar{Q}}_e(Q_d) = E\{Q|Q > Q_d\} = \int_{Q_d}^{\infty} Qp(Q)\,dQ \Big/ \int_{Q_d}^{\infty} p(Q)\,dQ,$$

or

$$\gamma_e Q_e = \int_{Q_d}^{\infty} Qp(Q)\,dQ, \tag{A 7}$$

where the implicit dependence of $Q_d$ is assumed. Similar expressions can be obtained for the non-turbulent class and higher-order moments, e.g. $\tilde{\bar{Q}}^2$ in the turbulent and non-turbulent regions, etc.

It is useful to examine the derivatives of the last two equations, which are

$$\frac{d\gamma_e}{dQ_d} = -p(Q_d), \quad \frac{d\tilde{\bar{Q}}_e}{dQ_d} = \frac{p(Q_d)}{\gamma_e}(\tilde{\bar{Q}}_e - Q_d). \tag{A 8), (A 9}$$

Using the definition of $\tilde{\bar{Q}}_e$, one can see that, within the range of interest, the sign of these derivatives can never change because $p(Q)$ can approach or equal zero only if the two classes are widely removed from each other. Such conditions are physically unrealizable in a continuum, although they could be found asymptotically if a discontinuity, such as a shock wave, were being studied. The consequence is that $\gamma_e$ and $\tilde{\bar{Q}}_e$ will be monotonic functions and there will not be any region where the intermittency or conditional averages of $Q$ will be independent of the threshold. This is quite important because in the past considerable effort has often been expended (unsuccessfully) looking for just such a region. Hence some other criteria must be used in order to determine a threshold value.

The technique used in this research is described by Chen (1975). Essentially it consisted of varying the threshold level over a large range of $Q$ that included the region where $p^n(Q) \cong 0$. In this region (A 8) and (A 9) become

$$\frac{d\gamma_e}{dQ_d} = -\gamma p^t(Q_d), \quad \frac{d\tilde{\bar{Q}}_e}{dQ_d} = \frac{\gamma p^t(Q_d)}{\gamma_e}(\tilde{\bar{Q}}_e - Q_d). \tag{A 10), (A 11}$$

The estimated values (with subscript $e$) could then be determined experimentally and this information used to find the correct values with the aid of the above equations.

The temperature signal $T(t)$ was used for $Q(t)$ in the present study. The variation of the parameters at a particular value of $y/\delta$ in the boundary layer are seen in figure 20. It is apparent that there is no plateau in $\gamma$ or the conditional averaged temperatures as discussed above. The estimated intermittency factor was linear over a broad range of the thresholds tested. As the threshold level approached the ambient temperature in the non-turbulent region, the slopes of all of the quantities changed dramatically. This was presumably due to the non-zero value of $p^n(T)$ in this region.

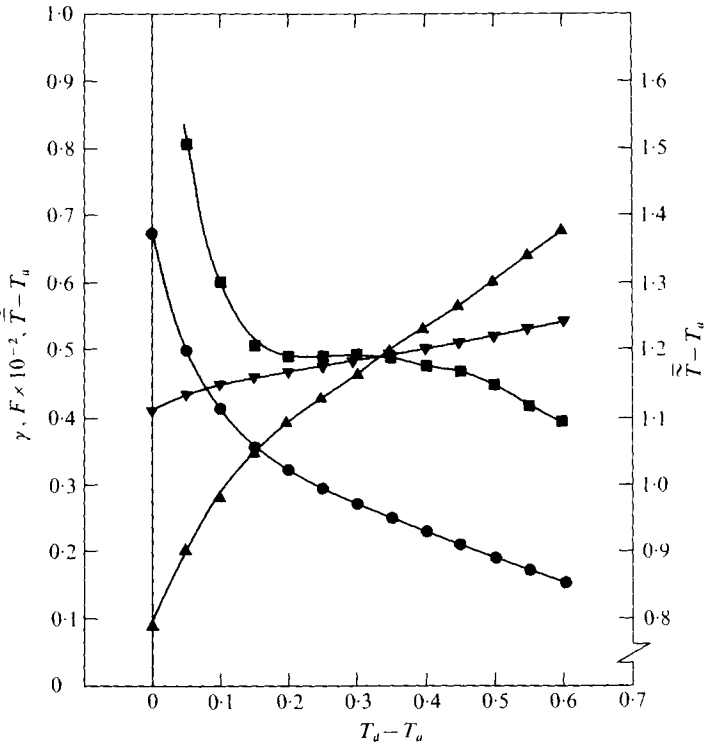


FIGURE 20. Variation of parameters as a function of the threshold level: ■, bulge crossing frequency, $F$; ●, intermittency factor, $\gamma$; ▼, non-turbulent zone average, $\widetilde{\widetilde{T}}-T_\infty$; ▲, turbulent zone average, $\widetilde{T}-T_\infty$. $T_a$ is the local ambient non-turbulent temperature.

Since the probability distributions do not contain any temporal information, alternative methods must be examined in order to determine the effect of the threshold level on the crossing frequency. Using (A 5), the estimated intermittency factor can be written as

$$\gamma_e(Q_d) = \lim_{\tau\to\infty} \int_0^\tau I(Q_d, t)\, dt.$$

Differentiating yields

$$\frac{d\gamma_e}{dQ_d} = \lim_{\tau\to\infty} \frac{1}{\tau} \int_0^\tau -\delta(Q_d - Q(t))\, dt$$
$$= -F(Q_d)\, S(Q_d),\dagger \qquad \text{(A 12)}$$

where $F(Q_d)$ is the bulge crossing frequency, given by

$$F(Q_d) = \lim_{\tau\to\infty} \frac{1}{\tau} \frac{N}{2}$$

and

$$S(Q_d) = \frac{2}{N} \sum_{n=1}^{N} \left| \frac{dQ(t)}{dt} \right|^{-1}_{t=t_n}.$$

† Using $\int_a^b f(x)\, \delta(g(x))\, dx = \sum_{n=1}^{N} \frac{f(x_n)}{|g'(x_n)|}$, where $g(x_n) \equiv 0$.

The total number of interface crossings is $N$, which is also a function of the threshold level. Similar expressions can be written down for the conditional averages. In order to have any physical significance, $F$ must be non-negative, as can be verified by using (A 8). However, no general criteria governing the variation of $F(Q_d)$ can be found. Since $F(Q_d)$ is a measure of the slope of $Q(t)$ at the threshold level, $F(Q_d)$ depends strongly upon the temporal form of $Q(t)$ and upon the threshold level. Hence $F(Q_d)$ is not necessarily a monotonic function as has been observed by Kibens *et al.* (1974) and will in general be more sensitive to the threshold level.

## REFERENCES


Antonia, R. A., Prabhu, A. & Stephenson, S. E. 1975 *J. Fluid Mech.* **72**, 455.

Bilger, R. W., Antonia, R. A. & Sreenivasan, K. R. 1976 *Phys. Fluids* **19**, 1471.

Blackwelder, R. F. 1977 *Phys. Fluids Suppl.* **20**, S 232.

Blackwelder, R. F. 1979 To appear in *Methods of Experimental Physics* (ed R. Emrich). Academic Press.

Blackwelder, R. F. & Kaplan, R. E. 1976 *J. Fluid Mech.* **76**, 89.

Blackwelder, R. F. & Kovasznay, L. S. G. 1972 *Phys. Fluids* **15**, 1545.

Brown, G. & Roshko, A. 1974 *J. Fluid Mech.* **64**, 775.

Chen, C. P. 1975 Ph.D. dissertation, University of Southern California.

Clauser, F. H. 1956 *Adv. Appl. Mech.* **4**, 1.

Corino, E. R. & Brodkey, R. S. 1969 *J. Fluid Mech.* **37**, 1.

Corrsin, S. 1943 *N.A.C.A. Wartime Rep.* W-94.

Corrsin, S. 1949 *N.A.C.A. Tech. Note* no. 1864.

Corrsin, S. 1957 *Proc. 1st Naval Hydr. Symp.* p. 373. Nat. Acad. Sci. Publ. SIS.

Corrsin, S. & Kistler, A. L. 1955 *N.A.C.A. Rep.* no. 1244.

Fulachier, L. 1972 D. Phys. Sci. thesis, Université de Provence.

Gupta, A. K. 1970 Ph.D. dissertation, University of Southern California.

Gupta, A. K., Laufer, J. & Kaplan, R. E. 1971 *J. Fluid Mech.* **50**, 493.

Hedley, T. B. & Keffer, J. F. 1974*a* *J. Fluid Mech.* **64**, 625.

Hedley, T. B. & Keffer, J. F. 1974*b* *J. Fluid Mech.* **64**, 645.

Johnson, D. S. 1959 *J. Appl. Mech.* **26**, 325.

Kaplan, R. E. & Laufer, J. 1969 *Proc. 12th Int. Cong. Appl. Mech., Stanford Univ.*, p. 236. Springer.

Kibens, V., Kovasznay, L. S. G. & Oswald, L. 1974 *Rev. Sci. Instrum.* **45**, 1138.

Kim, H. T., Kline, S. J. & Reynolds, W. C. 1971 *J. Fluid Mech.* **50**, 133.

Kline, S. J., Reynolds, W. C., Schraub, F. A. & Rundstadler, P. W. 1967 *J. Fluid Mech.* **30**, 741.

Kovasznay, L. S. G. 1970 *Ann. Rev. Fluid Mech.* **2**, 95.

Kovasznay, L. S. G. & Ali, S. F. 1974 *Proc. 5th Int. Heat Transfer Conf., Tokyo*, vol. 2, p. 99.

Kovasznay, L. S. G., Kibens, V. & Blackwelder, R. F. 1970 *J. Fluid Mech.* **41**, 283.

LaRue, J. C. & Libby, P. A. 1974 *Phys. Fluids* **17**, 1956.

Laufer, J. 1975 *Ann. Rev. Fluid Mech.* **7**, 307.

Laufer, J. & Badri Narayanan, M. A. 1971 *Phys. Fluids* **14**, 182.

Nychas, S. G., Hershey, H. C. & Brodkey, R. S. 1973 *J. Fluid Mech.* **61**, 513.

Offen, G. R. & Kline, S. J. 1974 *J. Fluid Mech.* **62**, 223.

Paizis, S. T. & Schwarz, W. H. 1974 *J. Fluid Mech.* **63**, 315.

Paizis, S. T. & Schwarz, W. H. 1975. *J. Fluid Mech.* **68**, 297.

Papailiou, D. D. & Lykoudis, P. S. 1974 *J. Fluid Mech.* **62**, 11.

Rao, N. K., Narasimha, R. & Badri Narayanan, M. A. 1971 *J. Fluid Mech.* **48**, 339.

ROCKWELL, D. O. & NICCOLS, W. O. 1972 *J. Basic Engng* **94**, 720.
THOMAS, R. M. 1973 *J. Fluid Mech.* **57**, 549.
WALLACE, J. M., BRODKEY, R. S. & ECKELMANN, H. 1977 *J. Fluid Mech.* **83**, 673.
WILLMARTH, W. W. 1975 *Adv. Appl. Mech.* **15**, 159.
WINANT, C. O. & BROWAND, F. K. 1974 *J. Fluid Mech.* **63**, 237.
ZARIC, Z. 1974 Etude statistique de la turbulence pariétale. *Rep. Boris Kidric Inst., Belgrade.*